

Modelling surface energy fluxes over maize using a two-source patch model and radiometric soil and canopy temperature observations

J.M. Sánchez^{a,*}, W.P. Kustas^a, V. Caselles^b, M.C. Anderson^a

^a *Hydrology and Remote Sensing Laboratory, USDA-ARS, Bldg. 007, BARC West, Beltsville, MD 20750, United States*

^b *Earth Physics and Thermodynamics Department, University of Valencia, C/Dr. Moliner, 50, 46100 Burjassot, Valencia, Spain*

Received 13 March 2007; received in revised form 18 July 2007; accepted 21 July 2007

Abstract

Models estimating surface energy fluxes over partial canopy cover with thermal remote sensing must account for significant differences between the radiometric temperatures and turbulent exchange rates associated with the soil and canopy components of the thermal pixel scene. Recent progress in separating soil and canopy temperatures from dual angle composite radiometric temperature measurements has encouraged the development of two-source (soil and canopy) approaches to estimating surface energy fluxes given observations of component soil and canopy temperatures. A Simplified Two-Source Energy Balance (STSEB) model has been developed using a “patch” treatment of the surface flux sources, which does not allow interaction between the soil and vegetation canopy components. A simple algorithm to predict the net radiation partitioning between the soil and vegetation is introduced as part of the STSEB patch modelling scheme. The feasibility of the STSEB approach under a full range in fractional vegetation cover conditions is explored using data collected over a maize (corn) crop in Beltsville Maryland, USA during the 2004 summer growing season. Measurements of soil and canopy component temperatures as well as the effective composite temperature were collected over the course of the growing season from crop emergence to cob development. Comparison with tower flux measurements yielded root-mean-square-difference values between 15 and 50 W m⁻² for the retrieval of the net radiation, soil, sensible and latent heat fluxes. A detailed sensitivity analysis of the STSEB approach to typical uncertainties in the required inputs was also conducted indicating greatest model sensitivity to soil and canopy temperature uncertainties with relative errors reaching ~30% in latent heat flux estimates. With algorithms proposed to infer component temperatures from bi-angular satellite observations, the STSEB model has the capability of being applied operationally. © 2007 Elsevier Inc. All rights reserved.

Keywords: STSEB; Soil temperature; Canopy temperature; Sensible heat flux; Latent heat flux

1. Introduction

The estimation of surface energy fluxes using remote sensing techniques has been widely studied in recent years. Despite some early criticisms suggesting that thermal infrared satellite observations are not sufficiently accurate for energy balance modelling (eg., Hall et al., 1992; Sellers et al., 1995), a wide variety of field experiments and associated studies have clearly shown the feasibility of using thermal remote sensing in the retrieval of surface fluxes (Anderson et al., 1997).

The development of two-source (soil+vegetation) layer models to accommodate partial canopy cover conditions

considers energy exchange between soil and canopy components, and hence interaction between soil and canopy elements (Choudhury & Monteith, 1988; Shuttleworth & Wallace, 1985). Another type of two-source model formulation is the so-called patch model where it is assumed that all the fluxes act vertically and that there is no interaction between soil and canopy components (i.e., a complete energy balance between the atmosphere and each element; Blyth & Harding, 1995; Lhomme & Chehbouni, 1999).

Norman et al. (1995) introduced a remote sensing-based two-source layer modelling framework for computing surface fluxes using directional brightness temperature observations. The Two-Source Energy Balance model (TSEB) was developed to require minimal inputs, similar to single-source models. Since typically only composite brightness temperature observations

* Corresponding author.

E-mail address: Juan.M.Sanchez@uv.es (J.M. Sánchez).

are available, an additional assumption is required for obtaining initial estimates of soil and vegetation canopy component temperatures and energy fluxes. For the TSEB scheme, the Priestley–Taylor (PT) equation applied to the vegetated canopy is used to obtain an initial solution. Although the TSEB uses the Priestley–Taylor approximation as an initial estimate for the canopy transpiration flux, the model has a built-in mechanism for throttling the PT coefficient, α_{PT} , back from its potential value (~ 1.3) when conditions of vegetation stress are detected (Kustas et al., 2004). The TSEB model has been widely applied, validated and modified to deal with unique landscapes over the past several years (French et al., 2003, 2005; Kustas & Norman, 1999a, 2000; Li et al., 2005; Schmugge et al., 1998).

Alternatively, if the partitioning of composite land-surface temperature into soil and canopy temperatures is known a priori, e.g., through dual angle Thermal InfraRed (TIR) decomposition (e.g., François, 2002; Otterman et al., 1992), the soil and canopy latent heat rates can be computed directly as a residual to the component energy budgets. In this case, the PT formulation is no longer required in the TSEB scheme (Kustas & Norman, 1997, 1999b).

In this paper a Simplified Two-Source Energy Balance (STSEB) model is developed, based on a patch representation of the energy exchange from soil and canopy, which permits estimation of surface fluxes under partial canopy cover conditions directly from component soil and canopy temperatures. A simple algorithm to predict the net radiation partitioning between soil and vegetation is also developed as part of the STSEB model.

Reliable measurements of the soil and canopy temperatures are required as inputs in the STSEB. These temperatures are not readily available from most satellite systems. Otterman et al. (1992) proposed one of the first models for inferring canopy and underlying soil temperatures from multi-directional measurements. Further studies on the angular effects on the brightness surface temperature for a variety of canopies (e.g., Chehbouni et al., 2001a; Lagouarde et al., 1995, 2000) were followed by new models to obtain soil and canopy temperatures from dual angle radiometric temperatures (François, 2002; François et al., 1997). Experiments using these dual angle observations of radiative surface temperature, in conjunction with energy balance models, to derive heat fluxes over partially vegetated surfaces have been conducted with varying degrees of success (Chehbouni et al., 2001b; Jia et al., 2003a; Kustas & Norman, 1997, 1999b; Merlin & Chehbouni, 2004). The Advanced Along-Track Scanning Radiometer (AATSR) on board the EOS-Terra satellite is currently able to provide quasi-simultaneous multispectral measurements at two view angles (approximately 0° and 53° at surface). Jia et al. (2003b) developed an operational algorithm to retrieve soil and canopy temperature over heterogeneous land surface based on the analysis of dual-angle and multi-channels observations made by the previous version of the AATSR, the second Along-Track Scanning Radiometer (ATSR-2).

The limitations and uncertainties in retrieving these component temperatures from the ATSR-2 observations indicate that the algorithm for retrieving the soil and canopy component temperatures, required as inputs in the STSEB

model, may be acceptable for operational applications using satellite observations. Kimes (1983) presented a strategy for obtaining component temperatures in a cotton row crop using multi-angle TIR measurements. He obtained root mean square deviation (RMSD) values of 1°C for the vegetation temperature and of 2°C for the soil temperature with respect to observed component temperatures. Chehbouni et al. (2001a,b) measured radiative temperature, over a grassland site, at two viewing angles mimicking nadir and forward observations of the AATSR. These authors concluded that an error of 1°C in measured directional radiative temperature leads to an error of about 1°C in the inverted component temperatures. Similar errors were obtained by Merlin and Chehbouni (2004). These authors inverted soil and canopy temperatures from simulations of directional temperature observations, yielding estimation errors in the range $1\text{--}2^\circ\text{C}$.

The objective of this paper is to validate the STSEB model under conditions of variable vegetation cover, as well as to explore its sensitivity to the input uncertainties likely to typically occur at regional scales. Ground and tower-based remote sensing, vegetation cover and micrometeorological data from maize (corn) crop in an experimental field site in Beltsville Maryland, USA during the 2004 summer growing season were used.

This paper is organized as follows. Section 2 provides the framework and details of the proposed STSEB model. A description of the study site and data used in this study are described in Section 3. An analysis of the radiometric temperatures and the energy balance measurements are given in Section 4. In Section 5, the results of a comparison between the surface energy balance components from the STSEB model and the observations as well as a STSEB–TSEB model inter-comparison are discussed. In addition, a sensitivity analysis of the STSEB model to uncertainties in key inputs is provided and the dependence on the fractional vegetation cover is also presented. Finally, conclusions are given in Section 6.

2. Model description

The net energy balance of soil–canopy–atmosphere system is given by (neglecting photosynthesis and advection):

$$R_n = H + LE + G + F \quad (1)$$

where R_n is the net radiation flux (W m^{-2}), H is the sensible heat flux (W m^{-2}), G is the soil heat flux (W m^{-2}), and F is the rate of change of heat storage in the canopy layer (W m^{-2}). For short canopies, F can be neglected since its contribution to energy balance is usually quite small and difficult to reliably estimate with standard micrometeorological measurements (Meyers & Hollinger, 2004; Wilson et al., 2002). The effective radiometric surface temperature in the same system, T_R (K), can be obtained as a weighted composite of the soil temperature, T_s (K), and the canopy temperature, T_c (K):

$$T_R = \left[\frac{P_v(\theta)\varepsilon_c T_c^4 + (1 - P_v(\theta))\varepsilon_s T_s^4}{\varepsilon} \right]^{1/4} \quad (2)$$

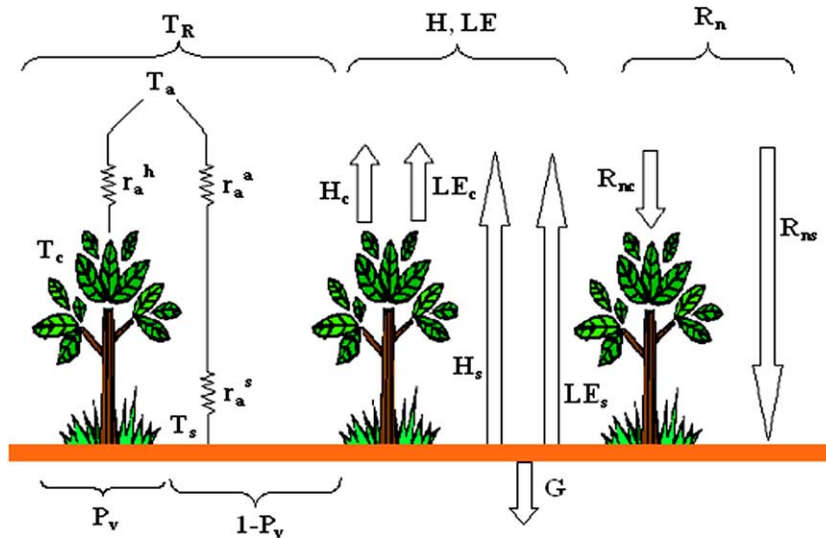


Fig. 1. Scheme of resistances and flux partitioning between soil and canopy, corresponding to the STSEB approach. Symbols are defined in the text.

where ε_c , and ε_s , are the canopy and soil emissivities, respectively, ε is the effective surface emissivity, and $P_v(\theta)$ is the fractional vegetation cover for the viewing angle θ . Note that Eq. (2) is based on the Stefan–Boltzmann law. Also, interaction between soil and canopy components (cavity effect) is not accounted for since preliminary calculations showed that it could be neglected for this work.

The angular vegetation cover fraction $P_v(\theta)$ can be estimated from the measurements of Leaf Area Index (LAI) via:

$$P_v(\theta) = 1 - \exp\left(\frac{-0.5\Omega(\theta)\text{LAI}}{\cos(\theta)}\right) \quad (3)$$

where $\Omega(\theta)$ is a clumping factor to characterize the heterogeneity of the surface (Anderson et al., 2005). This factor makes it possible to extend the typical equations for random canopies to heterogeneous cases. Lower values of Ω indicate stronger clumping, while $\Omega=1$ for a homogeneous canopy with a random dispersion of leaf area, and $\Omega>1$ indicates more regularized distributions. The clumping factor typically varies with the viewing angle, attaining a minimum value at nadir view (Ω_0). For a description of how to estimate Ω_0 from ground measurements of LAI, and the fractional amount of inter-row spacing covered by the crop canopy, see Li et al. (2005). The dependence of the clumping factor on θ can be estimated with:

$$\Omega(\theta) = \frac{\Omega_0\Omega_{\max}}{\Omega_0 + (\Omega_{\max} - \Omega_0)\exp(\kappa\theta^p)} \quad (4)$$

where Ω_{\max} approaches unity for an azimuth view perpendicular to the crop row, $p=3.8-0.46D$, D is the ratio between the canopy height and the nominal clump width, and k depends on stand architecture (Campbell & Norman, 1998). For azimuthal views perpendicular to the row, k can be obtained by the expression, $k=[0.3+(1.7\Omega_0)^{14}]$ (Anderson et al., 2005). Note that in row crops and other anisotropic stands, the clumping factor, and consequently the vegetation cover, will also vary azimuthally through the parameters k and Ω_{\max} . Anderson et al.

(2005) provides algorithms for estimating the expected variation of these parameters with azimuth angle.

The partitioning of the different fluxes into soil and canopy components was accomplished according to the scheme shown in Fig. 1. In the patch approach, an analogy between Ohm's law and the heat transfer equation shows that the magnitude corresponding to H is the current density (intensity per unit area). Therefore, according to this configuration, the addition between the soil and canopy contributions (values per unit area of component) to the total sensible heat flux, H_s and H_c , respectively, are weighted by their respective partial areas as follows (Lhomme & Chehbouni, 1999):

$$H = P_v H_c + (1 - P_v) H_s \quad (5)$$

where P_v (without a view angle argument) refers to the cover fraction at nadir view (i.e. $\theta=0^\circ$). In Eq. (5), H_s and H_c are expressed as:

$$H_c = \rho C_p \frac{T_c - T_a}{r_a^h} \quad (6a)$$

$$H_s = \rho C_p \frac{T_s - T_a}{r_a^a + r_a^s} \quad (6b)$$

where ρC_p is the volumetric heat capacity of air ($\text{J K}^{-1} \text{m}^{-3}$), T_a is the air temperature at a reference height (K), r_a^h is the aerodynamic resistance to heat transfer between the canopy and the reference height at which the atmospheric data are measured (m s^{-1}), r_a^a is the aerodynamic resistance to heat transfer between the point $z_{0M}+d$ (z_{0M} : canopy roughness length for momentum, d : displacement height) and the reference height (m s^{-1}), r_a^s is the aerodynamic resistance to heat flow in the boundary layer immediately above the soil surface (m s^{-1}). A summary of the expressions to estimate these resistances is shown in the Appendix. Eqs. (6a) and (6b) are taken from the parallel configuration of the TSEB model (Li et al., 2005;

Norman et al., 1995), modified to take into account the distinction between r_a^h and r_a^a .

To be consistent with the patch model configuration, a partitioning of the net radiation flux, R_n , between the soil and canopy is proposed as follows:

$$R_n = P_v R_{nc} + (1 - P_v) R_{ns} \quad (7)$$

where R_{nc} and R_{ns} are the contributions (values per unit area of component) of the canopy and soil, respectively, to the total net radiation flux. They are estimated by establishing a balance between the long-wave and the short-wave radiation separately for each component:

$$R_{nc} = (1 - \alpha_c)S + \varepsilon_c L_{sky} - \varepsilon_c \sigma T_c^4 \quad (8a)$$

$$R_{ns} = (1 - \alpha_s)S + \varepsilon_s L_{sky} - \varepsilon_s \sigma T_s^4 \quad (8b)$$

where S is the solar global radiation ($W m^{-2}$), α_s and α_c are soil and canopy albedos, respectively, σ is the Stefan–Boltzmann constant, and L_{sky} is the incident long-wave radiation ($W m^{-2}$).

A similar expression to Eq. (5) is used to combine the soil and canopy contributions, LE_s and LE_c , respectively, to the total latent heat flux:

$$LE = P_v LE_c + (1 - P_v) LE_s. \quad (9)$$

According to this framework, a complete and independent energy balance between the atmosphere and each component of the surface is established, from the assumption that all the fluxes act vertically. In this way, the component fluxes to the total latent heat flux can be written as:

$$LE_c = R_{nc} - H_c \quad (10a)$$

$$LE_s = R_{ns} - H_s - \frac{G}{(1 - P_v)}. \quad (10b)$$

Finally, G can be estimated as a fraction (C_G) of the soil contribution to the net radiation (Choudhury et al., 1987):

$$G = C_G (1 - P_v) R_{ns} \quad (11)$$

where C_G can vary in a range of 0.2–0.5 depending on the soil type and moisture. Recent studies have also expressed C_G as a function of time to accommodate temporal variation in this fraction (Santanello & Friedl, 2003).

The STSEB scheme is similar to a patch approach in that there is a real weighting of the soil and canopy elements and no direct coupling is allowed between soil and vegetation. Moreover, the current formulation for estimating the net radiation for soil and canopy is quite different from the common Beer's Law representation or the more physically-based two-stream layered approach proposed by Kustas and Norman (2000). The STSEB net radiation model does not consider attenuation of the downwelling sky and upwelling soil emission by an intervening canopy layer.

If T_s and T_c , can be estimated from directional measurements of T_R , or directly observed from appropriate measurements of the soil and canopy components, the system of equations in the STSEB can be solved without using the Priestley–Taylor approach to provide an initial estimate of LE_c . This proposed simplified approach (STSEB) is similar to a version of the TSEB model which also was modified to use directional radiometric temperature observations without the use of the PT assumption (Kustas & Norman, 1997, 1999b).

3. Study site and measurements

This work is based on the data registered in a corn crop field associated with the Optimizing Production Inputs for Economic and Environmental Enhancement (OPE3) program, located at the USDA-ARS Beltsville Agricultural Research Center, Beltsville, Maryland ($39^\circ 01'00''N$, $76^\circ 52'00''W$, 40 m above sea level). This site has four hydrologically bounded watersheds of approximately 4 ha each, which feed a wooded riparian wetland and first-order stream (Fig. 2a). For more information on the OPE3 experimental site see <http://www.ars.usda.gov/Research/docs.htm%3Fdocid%3D8438>. In this paper we will focus on the experimental campaign carried out in the summer of 2004, encompassing all the stages in the corn growing season, from the beginning of June (plant emergence) to the end of July (cob formation). Corn was planted on May 18th in rows (N–S orientated) of 76-cm spacing.

Starting on June 9th, soil and canopy radiometric temperatures were measured simultaneously using Apogee IRTS-P3 infrared radiometers¹. This radiometer has a broad thermal band (7–14 μm) with an accuracy of $\pm 0.3^\circ C$, and 37° field of view. Soil temperature was measured with an Infrared Thermometer (IRT) mounted in the center of a row at an oblique angle ($\sim 45^\circ$) viewing parallel to the row crop. It was placed at a height appropriate to ensure the view of just the soil space between rows. Canopy temperature was sensed with a second IRT placed within the row and oriented horizontally, viewing the plants parallel to the row orientation (Fig. 2b). The horizontal orientation ensured that this IRT was viewing only vegetation. Both temperature components were measured at two separated locations in the corn field, using two pairs of radiometers. Concurrently, the effective composite temperature of the corn + soil system was measured by a fifth IRT placed on a tower at 4.5 m height, viewing the surface at approximately a 45° viewing angle and an azimuth view perpendicular to the row direction. The micro-meteorological and eddy covariance instrumentation were mounted on the same 10-m tower (Fig. 2c).

Net radiation was measured with a Kipp & Zonen CNR-1 net radiometer at 4.5 m above ground level (agl). This net radiometer measures separately the incoming and outgoing shortwave and long-wave radiation components. Six REBS soil heat flow transducers (HTF-1) were buried 6-cm below the soil surface. Soil temperatures were measured at 2 and 4-cm depth by two Type-T soil thermocouples to compute the storage

¹ Trade and company names are given for the benefit of the reader and imply no endorsement by USDA.

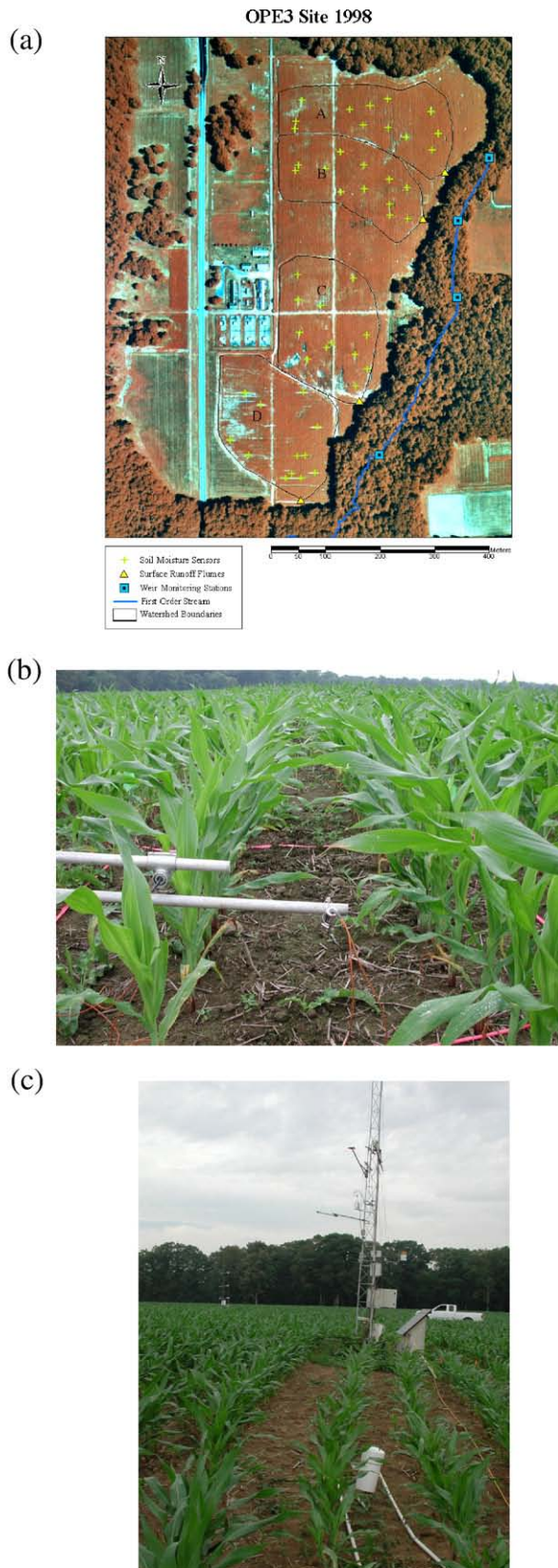


Fig. 2. (a) Aerial picture of the OPE3 study site. (b) Experimental assembly of two Apogee IRTS-P3 infrared radiometers to measure T_c and T_s . (c) General view of the target and the micro-meteorological tower on which the instrumentation was mounted.

component of the soil heat flux above the plates. A Campbell Scientific 3-D sonic anemometer and LiCor 7500 water vapour/carbon sensor positioned at 4-m agl was used to measure momentum, sensible heat, latent heat and carbon fluxes, as well as wind speed and direction. The eddy covariance instrumentation was oriented to the southwest, the predominant wind direction during the summer growing season. Unfavourable winds out of the north compromising the sonic measurements were flagged by the sensor system and discarded during post processing. Air temperature and vapour pressure was measured using a CSI HMP 45C sensor at 4-m agl. The sampling frequency was 10 Hz for the eddy covariance and 10 s for the energy balance and meteorological instrumentation. All data were stored as 30-minute averages on Campbell CR5000 and 23× data loggers.

Canopy geometry and LAI were sampled periodically during corn development. Measurements were made at multiple locations surrounding the tower and for the two sites where soil and canopy radiometric temperatures were being measured. Canopy height was sampled weekly, measuring 3 representative plants at each site to the height of the top leaves. The width of the vegetation clump across the row, used to compute the clumping parameter p in Eq. (4), was inferred from digital pictures taken above the target, using a digital analysis program. The LAI estimates were made using a LiCor LAI 2000 instrument. Finally, soil moisture was also monitored to better understand surface and subsurface soil water dynamics. Capacitance probes (EnvironSCAN, SENTEK), were used to measure volumetric water contents within a 10 cm radius from each sensor's center. The 2004 growing season was fairly wet, with volumetric water content values ranging between 12% and 27%.

4. Model input and validation data

4.1. Radiometric measurements

Ancillary measurements required to reliably estimate several key input variables to the STSEB model (i.e., radiometric soil and canopy temperatures and fractional cover) were analyzed and corrected for known errors.

The $P_v(\theta)$ values were estimated using Eqs. (3) and (4) as described in Section 2 with the necessary measurements needed to estimate the equation coefficients. A daily LAI value was interpolated from periodic measurements taken over the course of the experiment using a third order regression equation; this reproduced the expected phenological behaviour of LAI through the growth cycle (see Fig. 3a). A similar process was applied for reproducing the behaviour of canopy height from the periodic collected samples (see Fig. 3b). The clumping factor Ω (45°), associated with the view angle of the tower IRT measurement, was estimated via Eq. (4) using values of Ω_0 from Li et al. (2005) and Anderson et al. (2005), obtained over corn during the SMACEX-02 campaign in Iowa. Adjusting for the crop growth curves at OPE3 yielded Ω_0 values of 0.62, 0.70, 0.83, and 0.88 for the days of year 180, 186, 197, and 201, respectively. Daily values of Ω_0 were linearly interpolated between these values. Fig. 3c shows the time-evolution of the

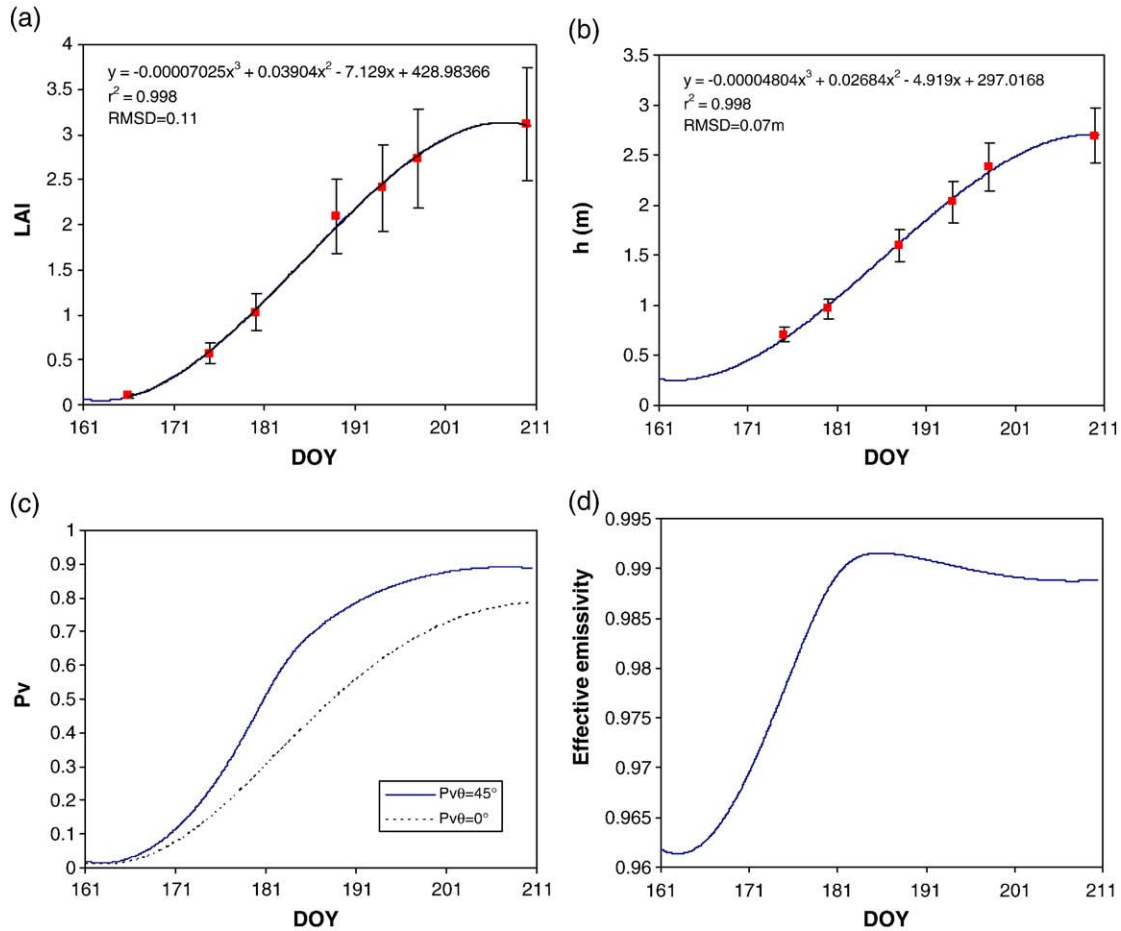


Fig. 3. (a) LAI evolution during the experiment, points correspond to sample measurements with an uncertainty of 20% whereas the line represents the regression of those points. (b) Canopy height evolution during the experiment, points correspond to sample measurements with an uncertainty of 10% whereas the line represents the regression of those points. (c) Evolution of the modelled $P_v(\theta)$ during the experiment, for both $\theta=0^\circ$ and $\theta=45^\circ$. (d) Evolution of the effective surface emissivity during the experiment.

vegetation cover fraction values, $P_v(0^\circ)$ and $P_v(45^\circ)$ during the experiment.

Accurate measurements of both T_c and T_s , and the vertical gradients with respect to the reference air temperature are crucial for a correct partitioning of the surface fluxes from soil and canopy components. For the canopy component, these gradients are often less than 1 °C. Consequently, radiometric canopy temperatures must be determined with a relatively high level of accuracy. As a first step, all the Apogee IRT measurements were corrected to add thermal mass, using a sensor body temperature, according to the procedure outlined by Bugbee et al. (1999). Then, the radiometric temperatures were corrected for emissivity and atmospheric effects using the radiative transfer equation, adapted to ground measurements. The remotely measured radiance values in channel i of a radiometer at an observation angle θ , $R_i(\theta, h)$, consist of two main contributions: (1) the radiance at surface level, which is attenuated by the absorption of the atmosphere between the surface and the instrument, characterized by the atmospheric transmittance and (2) the path radiance emitted by the atmosphere in the viewing direction. Due to the short atmospheric path between the surface and the sensor in our cases, the path radiance is negligible and the atmospheric

transmissivity is equal to one. Consequently, the radiance measured by a ground radiometer can be considered directly as:

$$R_i(\theta, h) = \varepsilon_i(\theta)B_i(T) + [1 - \varepsilon_i(\theta)]L_{i \text{ atm hem}}^\downarrow \quad (12)$$

where $B_i(T)$ is the Planck's function for a temperature T , $\varepsilon_i(\theta)$ is the i channel emissivity and $L_{i \text{ atm hem}}^\downarrow$ is the hemispheric downwelling sky irradiance divided by π (Lambertian reflection assumed).

Atmospheric profiles from radiosoundings launched in an area nearby the study site were used in the MODTRAN 4 code (Berk et al., 1999) to estimate the downwelling sky radiance for the atmospheric correction. Values of $\varepsilon_c=0.985\pm 0.011$ and $\varepsilon_s=0.960\pm 0.013$ were used to estimate T_c and T_s , respectively (Rubio et al., 2003). Some authors, such as Mira et al. (in press), have shown that soil emissivity can vary with soil moisture. However, a constant value of ε_s was used in this work since the maximum difference calculated in its value (using the relationships derived in Mira et al. (in press)), consequence of the soil moisture variation during the experiment, was very similar to the estimation error of 0.013, obtained by Rubio et al. (2003). To obtain values of T_c and T_s that are more representative of the

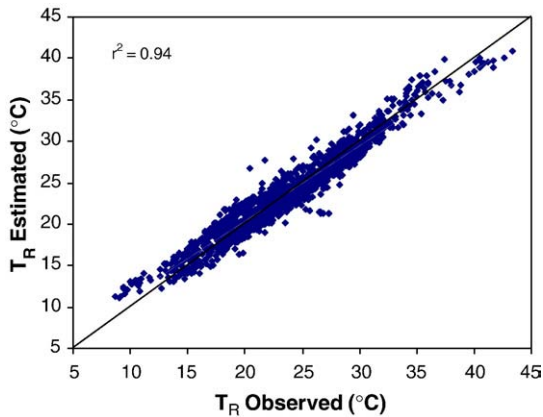


Fig. 4. Linear regression between T_R estimated by Eq. (2) from the measurements of T_c and T_s versus the direct observations from the tower.

whole corn field, averages between the two different measurement locations were used.

From a modelling standpoint, the vegetation–soil system can be described as consisting of five basic components: the top, shaded canopy, shaded soil, sunlit canopy, and sunlit soil. Thus, the radiance reaching a sensor placed at the top of the system is the weighted sum of the radiances coming from the different parts. Caselles et al. (1992) developed a theoretical model describing the relationship between the effective temperature of the radiative vegetation–soil system and the temperature of each component, depending on the proportions of each component, their emissivities, and the crop structure. These authors used an Everest Model 210 broadband radiometer, with an instantaneous field of view (IFOV) of 2° , to validate the proposed model over an orange grove. Model validation was carried out in the case corresponding to vertical observation, yielding a standard error of estimate about 1°C with an underestimation of 0.2°C .

For the current experiment, the corn–soil system was reduced to only two components since it was assumed that the wide field of view of the Apogee radiometers ($\sim 40^\circ$), and the deployment configuration, sampled effective values of the soil and canopy temperatures, weighting for the sunlit and shaded portions (Note that the impact of the diurnal variations in the ratio of sunlit/shaded leaves viewed by the canopy IRT cannot be accounted with the measurement design used in the experiment.). The reliability of these soil and canopy temperature components was evaluated by computing an effective surface temperature via Eq. (2) and comparing to the composite target radiometric temperatures measured from the tower. The tower radiometric temperatures were also corrected of atmospheric and emissivity effects. In this case, the emissivity of the target observed by the radiometer depends on the vegetation cover fraction and was estimated as a combination of ε_c , ε_s , and a cavity term accounting for the multiple reflections inside the canopy structure. The method proposed by Valor and Caselles (1996) was used to determine the effective surface emissivity ($\varepsilon = \varepsilon_c P_v(\theta) + \varepsilon_s(1 - P_v(\theta))(1 - 1.74P_v(\theta)) + 1.7372P_v(\theta)(1 - P_v(\theta))$). Fig. 3d shows the evolution of the value of this effective surface emissivity during the campaign.

In Fig. 4 T_R estimated from the measurements of T_c and T_s is compared to direct observations from the tower-based radiom-

eter. A standard error of $\pm 1.4^\circ\text{C}$ and a bias of 0.02°C were obtained, with a slight tendency to overestimate the low T_R values and to underestimate the high values. Even though the standard error is greater than that found by Caselles et al. (1992), the agreement is acceptable, particularly if we consider the significant variation in environmental and canopy cover conditions that existed over the two month period of observation. Moreover, the flux tower was located 10s of meters from the radiometers viewing the soil and canopy components. Consequently, slight discrepancies in the effective temperatures, due to differences in the fractional cover and surface soil moisture conditions between the two sites will contribute to the scatter observed. Also, note that T_c and T_s were observed parallel to the row crop whereas T_R was sensed at a perpendicular view, which is likely to affect the level of agreement one could expect from this type of comparison. Given these uncertainties, these results support the assumption that temperature components, T_c and T_s , from the radiometric observations are representative of the effective soil and canopy temperatures in the flux footprint area surrounding the tower and thus can be employed with the STSEB model for computing the fluxes. In future field experiments the decomposition of dual-angle IRT measurements for inferring soil and canopy temperature components will be evaluated and resulting flux estimation using the STSEB model will be assessed.

4.2. Flux measurement uncertainty

A lack of the energy balance closure has been observed in numerous eddy covariance studies conducted over different landscapes. Possible causes of observed energy imbalances include instrumental effects, corrections applied when post-processing of the turbulence data, the length of the sampling interval, and the heterogeneity of the landscape (Foken et al., 2006; Lamaud et al., 2001; Laubach & Teichmann, 1999; Meyers & Hollinger, 2004; Wilson et al., 2002). Analysis of the energy balance over corn crops has shown closure ratios around 0.8 (Prueger et al., 2005), although 0.9 is attainable (Meyers & Hollinger, 2004). In Fig. 5 a linear regression between R_n and the sum $H+LE+G$ from Eq. (1) for the OPE3 dataset yields a slope ~ 0.9 , which indicates approximately 10% of the estimated available energy is not accounted for, on average.

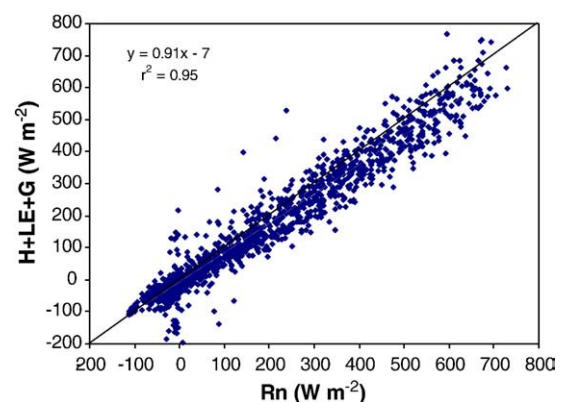


Fig. 5. Linear regression between the two terms of the Energy Balance Equation.

Table 1
Statistical analysis of the STSEB model performance with the full OPE3-2004 dataset (daytime+nighttime)

Flux	Bias ^a (W m ⁻²)	RMSD ^b (W m ⁻²)	MAD ^c (W m ⁻²)	a ^d	b ^e (W m ⁻²)	r ^{2f}
R _n	3	13	9	1.02	0.06	0.997
G	20	38	30	0.70	24	0.767
H _{EC}	-1.7	19	13	0.77	3	0.749
H _{BR}	-8	24	16	0.68	1.5	0.719
LE _{EC}	5	61	48	1.20	-15	0.863
LE _{RE}	-15	48	40	1.10	-27	0.919
LE _{BR}	-7	48	39	1.11	-22	0.914

H_{EC} and H_{BR} are the sensible heat fluxes measured by eddy-correlation and calculated by conserving the measured Bowen ratio, respectively. LE_{EC}, LE_{RE} and LE_{BR} are the latent heat fluxes measured by eddy-correlation, and obtained using residual method and Bowen ratio method as closure, respectively.

^a Bias: $BIAS = \sum_{i=1}^n (P_i - O_i)/n$.

^b Root Mean Square Difference: $RMSD = \left[\sum_{i=1}^n (P_i - O_i)^2/n \right]^{1/2}$.

^c Mean Absolute Difference: $MAD = \sum_{i=1}^n |P_i - O_i|/n$.

^d Slope of the linear regression: $P_i = aO_i + b$.

^e Intercept of the linear regression: $P_i = aO_i + b$.

^f Determination coefficient.

where P_i and O_i are the predicted and observed variables, respectively.

*Error values are shown with two significant figures in order to allow further analysis and comparisons.

Twine et al. (2000) suggested two methods to enforce the energy balance closure, namely by calculating the latent heat flux as a residual of the energy balance (RE method), and by conserving the measured Bowen ratio (BR method). In the RE method, the direct eddy-covariance measurements of H are assumed reliable and lack of closure is largely due to an under-measurement of LE. In the BR method, it is assumed both turbulent fluxes are under measured with the amount distributed between H and LE based on the Bowen ratio (H/LE), which defines the fraction of available energy going into sensible versus latent heat. Since there is no consensus on how to resolve lack of energy balance closure with eddy covariance, comparison between model estimations and ground observations will be performed without closure, and enforcing closure using both the RE and BR techniques.

5. Results and discussion

5.1. Validation of the STSEB model

Almost 1700 observations, without any exclusion related to time of day or sky conditions, were used to run and evaluate STSEB model output. The statistical results of the model-measurement comparisons for diurnal fluxes are listed in Table 1. The errors deteriorate slightly when only daytime values (when R_n>0) are considered (Table 2), as modelled nighttime flux estimates are constrained to be near zero. The daytime flux statistics, however, are more descriptive of overall model utility and therefore these are discussed in the text below.

For estimating net radiation, Eqs. (7), (8a) and (8b) were applied using values of α_s=0.12, α_c=0.20, ε_s=0.960, and ε_c=0.985, characteristic of a corn canopy (Campbell & Norman, 1998). The model reproduces measured net radiation with good accuracy, yielding a bias of 8 W m⁻², and RMSD=18 W m⁻²

(Fig. 6a). A constant value of C_G=0.35 was used in Eq. (11), corresponding to the midpoint between its likely limits (Choudhury et al., 1987). Similar values have been assigned to this constant in recent works under similar conditions (Li et al., 2005). Soil heat flux results overestimate measurements by 17 W m⁻² on average, with RMSD=43 W m⁻² (Fig. 6b). Calibration of the C_G value for this site would improve the agreement; however the purpose of this study was not to tune the model to this specific site but to evaluate its generality.

Tables 1 and 2 list statistics comparing turbulent fluxes estimates of H and LE with the eddy covariance fluxes in their original form (EC), and corrected for closure using the residual (RE) and Bowen ratio (BR) techniques. The RE closure technique, using H_{EC} and assigning all closure error to LE (LE_{RE}), yields the best agreement between STSEB and measured fluxes. Several studies with the TSEB model have also found optimal agreement using the RE method (e.g., Li et al., 2005).

Model comparisons with H_{EC} and LE_{RE} are shown in Fig. 6c–d. After correcting the aerodynamic resistances for atmospheric stability, as described in the Appendix, H was estimated via Eqs. (5), (6a), and (6b). Comparisons between modelled and measured H show a negative bias of -3 W m⁻², and an RMSD of 22 W m⁻² (Fig. 6c). The slope (a) of a linear regression between STSEB H and H_{EC} is 0.86, indicating that the bias is multiplicative. The bias is further exacerbated when the Bowen ratio closure technique is applied, yielding a=0.76.

For LE obtained by using Eqs. (9), (10a), and (10b), there is a tendency to overestimate the observed latent heat flux, LE_{EC} with a slope of 1.04 and an RMSD=62 W m⁻². As indicated in Section 4.2, this overestimation may be due in part to an under-measurement problem with the eddy covariance system. The agreement of the LE results improves significantly when the RE closure technique is applied to the observations, decreasing the slope to 0.98 and the RMSD to 51 W m⁻² (see Fig. 6d and Table 2). If energy closure is enforced by the Bowen ratio technique (LE_{BR}), a similar slope is obtained (a=1.00), but now with a null bias and an RMSD of 49 W m⁻² (see Table 2).

Under conditions of very low and very high vegetation cover, the scene is relatively homogeneous, and the STSEB model formulation should approximate a single source evaluation. However, under high cover, observations of T_s will be ill-constrained, whereas T_c is difficult to measure accurately under near-bare-soil conditions. To assess the performance of the STSEB under these potentially challenging limiting conditions,

Table 2
Statistical analysis^a of the STSEB model performance with the daytime OPE3-2004 dataset

Flux	Bias ^a (W m ⁻²)	RMSD ^b (W m ⁻²)	MAD ^c (W m ⁻²)	a ^d	b ^e (W m ⁻²)	r ^{2f}
R _n	8	18	13	1.01	5	0.992
G	17	43	31	0.66	35	0.620
H _{EC}	-3	22	16	0.86	3	0.746
H _{BR}	-10	26	19	0.76	2	0.738
LE _{EC}	29	62	49	1.04	22	0.820
LE _{RE}	-6	51	40	0.98	-2	0.849
LE _{BR}	0	49	40	1.00	0.6	0.854

^a See Table 1 for column definitions.

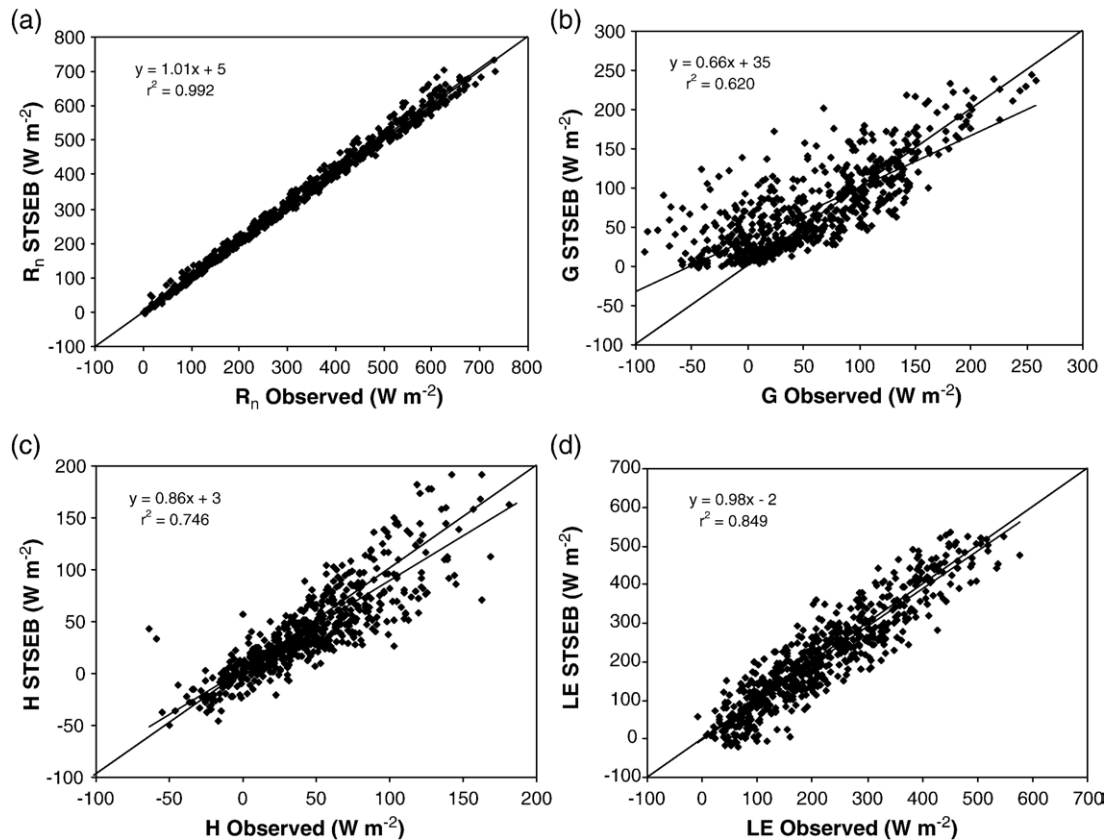


Fig. 6. Linear regressions between the surface energy fluxes estimated by the STSEB model versus their corresponding ground measured values: (a) R_n , (b) G , (c), H (eddy-covariance measurements), (d) LE (RE technique applied).

the experiment reported above was repeated considering only the period when $0.05 < P_v < 0.75$. No significant improvement in the results for the STSEB validation was observed for this restricted time period, suggesting that the performance of the STSEB model does not degrade under low and high vegetation cover conditions.

5.2. Comparison with the TSEB model

To assess the impact of the simple patch approach used in the STSEB model in comparison with the layer configuration in the TSEB model, the TSEB was also applied to the OPE3 dataset from 2004. The TSEB was restructured as described by Kustas and Norman (1997) to operate similarly to the STSEB, using observed values of soil and canopy component temperature and thereby eliminating the need for an initial PT approximation for potential canopy transpiration.

Statistics comparing this version of the TSEB (TSEB_comp) with observed daytime fluxes (corrected for closure using the residual method) are provided in Table 3, and graphical comparisons of flux components estimated by the STSEB and TSEB_comp models are shown in Fig. 7. In general, there is good agreement between STSEB and TSEB_comp output (Fig. 7) as well as similar statistical results with the flux observations (cf. Tables 2 and 3). Most notable are the differences in modelled sensible heat flux, shown in Fig. 7c. For low values of P_v , i.e., when soil component predominates in

the scene, the STSEB model tends to compute higher values of H compared to TSEB, while it estimates lower H -values for high vegetation cover conditions (when the predominant component is the vegetation canopy elements). The agreement in model output as well as with flux observations suggests that the simple patch formulation for net radiation contained in the STSEB model, performs almost as well as the more detailed two-stream representation in the TSEB_comp under this set of conditions. It appears the patch modelling scheme is appropriate under the set of environmental conditions analyzed in this study.

5.3. Sensitivity analysis of the STSEB model

In the validation study discussed in Section 5.1, the STSEB model was tested with input data that were acquired in situ, ensuring that these inputs were representative of local

Table 3
Statistical analysis^a of the TSEB_comp model performance with the daytime OPE3-2004 dataset

Flux	Bias ^a ($W m^{-2}$)	RMSD ^b ($W m^{-2}$)	MAD ^c ($W m^{-2}$)	a^d	b^e ($W m^{-2}$)	r^{2f}
R_n	-2	11	8	0.97	8	0.997
G	17	38	29	0.67	35	0.713
H_{EC}	-13	25	19	0.73	-1.7	0.737
LE_{RE}	-5	43	34	0.93	9	0.879

^a See Table 1 for column definitions.

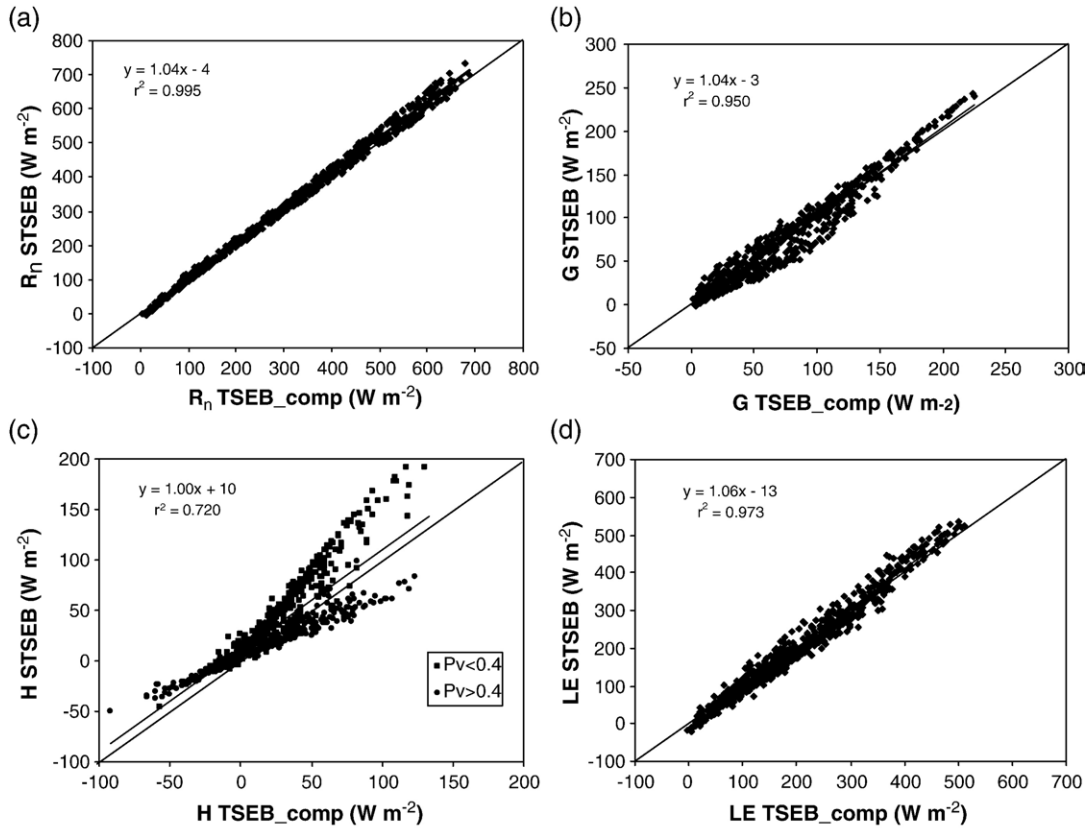


Fig. 7. Linear regressions between the surface energy fluxes estimated by the STSEB model versus the results of the TSEB_comp model: (a) R_n , (b) G , (c) H , (d) LE .

conditions. For operational monitoring over regional scales, using satellite-derived inputs and non-local meteorological data, the typical uncertainties in the inputs for STSEB may lead to significant errors in estimated fluxes. To assess the impact of typical errors in remotely derived model inputs, a sensitivity analysis of the STSEB approach was performed following the method suggested by Zhan et al. (1996). The relative sensitivity, S_p , of a model flux estimate, Z , to X uncertainties in a parameter p , can be expressed as:

$$S_p(X) = \left| \frac{Z_- - Z_+}{Z_0} \right| \quad (13)$$

where Z_0 , Z_+ , and Z_- are the fluxes (H , R_n , or LE) predicted when p equals its reference value p_0 , when p is increased by X its reference value, and when p is decreased X its reference value, respectively, with all other input parameters held constant at their reference values. This type of sensitivity analysis will not address multiple input uncertainties that might cause cumulative errors. In other cases, errors in several of the inputs may tend to cancel out, reducing the overall error in the flux estimates.

Several sensitivity studies have been performed with the TSEB model (Anderson et al., 1997; Kustas & Norman, 1997; Zhan et al., 1996). Each of these studies tested model sensitivity under a single scenario, with one set of input reference values. However, as pointed out by Zhan et al. (1996), the S_p value

computed for a given input may depend on the choice of the reference value for that input. In this analysis, all hourly daytime data were used as sets of reference values; hence a wide range of input values were considered. For each input variable, the time-series simulation was then performed using perturbed values of that variable, and S_p was averaged over the entire time series.

A list of all variables and parameters required by the STSEB model, as well as their assigned uncertainties, are provided in Table 4. Typically, a range of variation in the inputs of $\pm 10\%$ has been assumed in the sensitivity analysis of the two-source models (e.g., Anderson et al., 1997; Zhan et al., 1996). However, this assumed uncertainty might be unrealistic for some inputs such as temperatures or emissivity values (Coll et al., 2003, 2005; Valor & Caselles, 1996), while it might be too conservative for others such as LAI or clumping factor (Anderson et al., 2004). The variation in T_s was assigned twice the range of uncertainty in relation to T_c in order to incorporate the typically greater effect of the atmospheric and emissivity correction to the soil component. For air temperature, the uncertainty reflects typical errors associated with spatially interpolating observations from a weather station network. For the solar and incident long-wave radiation the uncertainty was reduced to $\pm 5\%$ due to the relatively spatial homogeneity these parameters show at a regional scale. Relative sensitivity values, S_p , estimated for some of these parameters can be artificially high in the case of H , due to low values of the reference flux. Since a major objective is in

Table 4
Average values of the relative sensitivity, S_p , of the STSEB model to the uncertainties, X , in the required inputs for estimating H , R_n , and LE (description of results in italics in the manuscript)

INPUT	T_c (°C)	T_s (°C)	T_a (°C)	u (m s ⁻¹)	S (W m ⁻²)	L_{sky} (W m ⁻²)	LAI	Ω_0	h (m)	z'_0 (m)	z' (m)	α_c	α_s	ε_c	ε_s
X	1 °C <i>0.5 °C</i>	2 °C <i>1 °C</i>	1 °C <i>0.2 °C</i>	10%	5%	5%	20%	20%	10%	50%	50%	20%	20%	0.02	0.02
H	0.66 <i>0.45</i>	0.86 <i>0.49</i>	1.10 <i>0.28</i>	0.17	0.0018	0.0018	0.08	0.07	0.10	0.03	0.09	<10 ⁻³	<10 ⁻³	0.24	0.23
R_n	0.015 <i>0.008</i>	0.05 <i>0.03</i>	0 <i>0</i>	0	0.12	0.13	0.008	0.008	0	0	0	0.04	0.04	0.003	0.007
LE	0.10 <i>0.06</i>	0.23 <i>0.11</i>	0.17 <i>0.04</i>	0.04	0.14	0.15	0.03	0.03	0.018	0.008	0.02	0.05	0.05	0.04	0.05

modelling vegetation stress and water use, the analysis also considered the sensitivity of R_n and LE to input errors.

Average S_p values for the whole experimental period are listed in Table 4 for the three fluxes, with values greater than 10% denoted in bold to indicate parameters that have a significant effect on the flux retrieval. Errors in soil, canopy, and air temperatures clearly have the greatest impact on the modelled sensible heat flux. Uncertainty in other parameters such as soil and canopy emissivity values, canopy height, or wind speed also have a measurable effect on H . For R_n , incoming shortwave and long-wave radiation are the key inputs that lead to sensitivities greater than 10%. These radiation inputs, together with the soil, canopy and air temperatures, have the greatest effect on LE retrieval. For LE, all inputs have S_p values below 25% on average. The sensitivity of the STSEB model to z'_0 and z' is not significant compared to other inputs, despite the high uncertainty values assumed (Sauer et al., 1995).

Sensitivities associated with the local validation experiment reported in Section 5.1 are considerably lower than those expected for remotely driven experiments. In Table 4, entries in italics indicate typical errors associated with input values measured locally, using IRTs and local meteorological towers. For the soil and canopy temperatures, the assigned uncertainties reflect expected errors in atmospheric and emissivity corrections to the observed uncorrected brightness temperatures acquired with ground-based radiometers. With a local meteorological tower, significantly less uncertainty is likely in T_a (~0.2 °C). Sensitivity values, considering these lower uncertainties in temperature inputs, are also included in Table 4 (in italics).

Fig. 8 shows variations in model sensitivity with fractional vegetation cover condition, a dependence that is rarely reported in the literature. Because the reference data used in this sensitivity analysis were collected over the whole growing season, model uncertainty as a function of P_v can be investigated. The S_p data were grouped in eight bins of width 0.1 in P_v , giving a range from 0.1 to 0.8. Average relative sensitivity values were computed for each P_v bin. Results for H , R_n , and LE are plotted in Fig. 8a–c, respectively. Inputs with S_p values lower than 0.03 are not shown.

For model inputs related to the soil (T_s , α_s , and ε_s), S_p decreases as P_v increases, whereas for those directly related with the canopy, such as T_c , α_c , and ε_c , an increase in S_p is observed. For variables related to canopy structure such as LAI, canopy height and clumping, the relative sensitivity also increases as a function of P_v . Sensitivities to errors in incoming shortwave and long-wave radiation show no significant dependence on P_v .

For latent heat flux estimation under low vegetation cover conditions ($P_v < 0.2$), the STSEB model is most sensitive to uncertainties in T_s , and under high vegetation cover conditions

($P_v > 0.6$) to uncertainties in T_c and T_a (Fig. 8c). The sensitivity of the STSEB model to any of the assumed uncertainties in the required inputs for the LE retrieval is less than 35% for the whole range of P_v . The sensitivity is even lower for the fractional vegetation cover range $0.3 < P_v < 0.6$, which yields S_p values less than 20%. Simulations in the estimation of soil and canopy temperatures from directional radiative temperature observations performed by François (2002) covering a wide range of vegetation cover and moisture conditions showed that

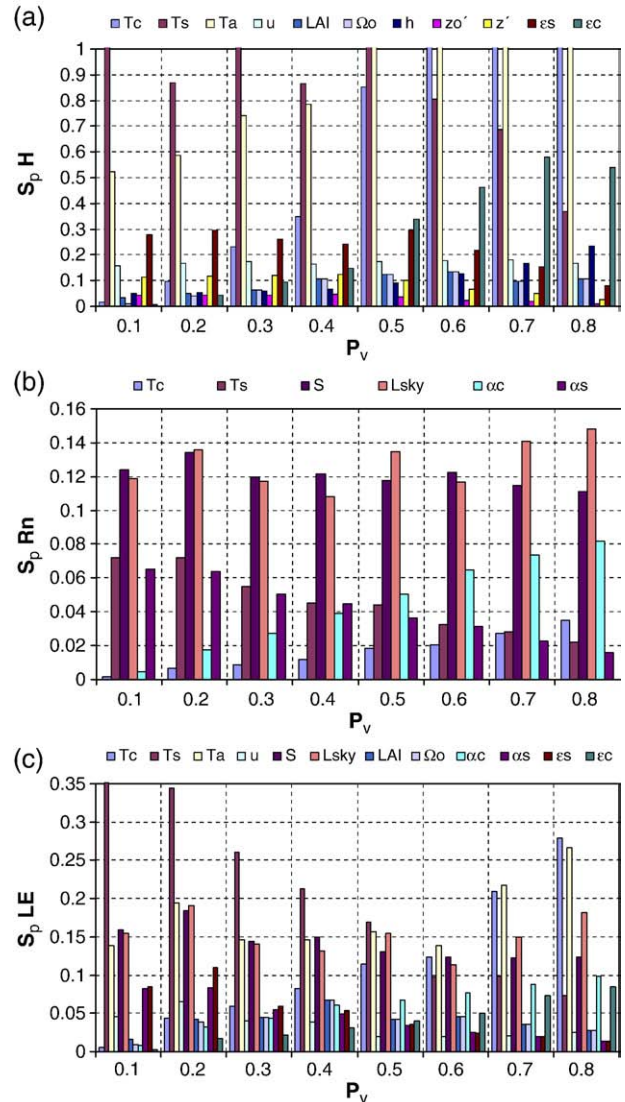


Fig. 8. Evolution of the relative sensitivity of the STSEB model to the different required inputs, S_p , with the vegetation cover, P_v , for: (a) H (Note that S_p scale has been limited to 1 in order to provide overall clarity), (b) R_n , (c) LE.

the error on T_s retrieval increases with increasing LAI, while the error on retrieved T_c generally decreases. If this behaviour were taken into account, the estimated uncertainties in the flux estimates might be reduced.

6. Conclusions

A Simplified Two-Source Energy Balance model (STSEB) has been proposed to estimate surface fluxes over sparse canopies from the radiometric soil and canopy temperatures. The advantage of the present patch modelling approach is that it is a simplified version of the TSEB model, particularly in the way the net radiation is partitioned between the soil and vegetation. On the other hand, the STSEB requires input measurements of canopy and soil temperature, while the TSEB performs an internal decomposition of a bulk surface radiometric temperature observation. The STSEB model has been tested under a full range of crop cover conditions using field data from a corn field at the USDA-ARS OPE3 experimental site in Beltsville Maryland, USA.

Radiometric soil and canopy temperatures were measured separately, and their reliability as representative component temperatures to be used as input to the STSEB model has been evaluated by comparing an independent tower-based radiometric temperature measurement of the effective composite temperature with that estimated from the two components. An RMSD = ±1.4 °C between these two estimates of the effective composite temperature was observed.

The validation of the STSEB approach, using measurements of daytime surface energy fluxes, yields errors between 15 and 50 W m⁻² for R_n , G , H , and LE after correcting the observed fluxes for closure. Reasonable agreement was obtained between the STSEB and a version of the TSEB model constructed to use component temperature data.

The operational capability of the STSEB model has been explored by means of an analysis of the sensitivity of the model flux output to uncertainties in the required inputs. The input temperature data, T_c , T_s , and T_a are shown to have the greatest impact on the STSEB estimate of the fluxes. Under the conditions considered in this study, much of the available energy was converted to latent heat, LE. As a result, the sensitivity of the STSEB model output in H to uncertainties in air, soil and canopy temperatures often exceeded 100% of its reference value. On the other hand, sensitivity of the STSEB model output in LE to these temperature uncertainties was generally less than 30% and not strongly a function of the vegetation cover over the range $0.1 < P_v < 0.8$.

In summary, these results demonstrate the utility of the STSEB model for a corn crop over a full range in cover conditions when reliable measurements of soil and canopy temperatures are available. Further field studies are needed to assess the utility of the STSEB model over different land cover types, particularly under drier conditions where the sensible heat flux represents a significantly greater proportion of the available energy (i.e., net radiation less soil heat flux). More importantly there is a need to further assess whether the STSEB approach is robust and comparable to the TSEB model and other schemes developed to use dual-angle satellite based

radiometric temperature observations with algorithms such as the one proposed by Jia et al. (2003b) to infer soil and canopy temperature components.

Acknowledgements

This work was funded by the *Ministerio de Educación y Ciencia* (Project CGL2004-06099-C03-01, co-financed with European Union FEDER funds, *Acciones Complementarias* CGL2005-24207-E/CLI and CGL2006-27067-E/CLI), and the University of Valencia (*V Segles* Research Grant of Mr. J. M. Sánchez). The authors would like to thank the logistical support in operating and maintaining the OPE³ site as well as data collection and archiving efforts of Drs. Craig Daughtry, Timothy Gish and Greg McCarty of the USDA-ARS Hydrology and Remote Sensing Lab. The micrometeorological tower data and vegetation were made available through the efforts of technician Mr. Andrew Russ of the Hydrology and Remote Sensing Lab and Dr. John Prueger from the USDA-ARS Soil Tilth Lab in Ames, Iowa. Funds from the USDA-ARS Hydrology and Remote Sensing Lab help support Mr. J. M. Sánchez as a visiting scholar.

Appendix A. Expressions to estimate the aerodynamic resistances in the STSEB approach

The aerodynamic resistances used for this work are based on the general framework described in Norman et al. (1995), Kustas and Norman (1999a) and Li et al. (2005), and adapted to modifications proposed by Brutsaert (1999). The aerodynamic resistance to heat transfer between the canopy and the reference height (z), r_a^h , is expressed as follows:

$$r_a^h = \frac{\left[\text{Ln} \left(\frac{z_u - d}{z_{0M}} \right) - \Psi_M \left(\frac{z_u - d}{L} \right) + \Psi_M \left(\frac{z_{0M}}{L} \right) \right] \left[\text{Ln} \left(\frac{z_T - d}{z_{0H}} \right) - \Psi_H \left(\frac{z_T - d}{L} \right) + \Psi_H \left(\frac{z_{0H}}{L} \right) \right]}{k^2 u} \quad (\text{A1})$$

where, z_u and z_T are the measurement heights (m) for wind speed, u (m s⁻¹), and air temperature, respectively, d is displacement height (m), z_{0M} is the canopy roughness length for momentum (m), z_{0H} is the canopy roughness length for heat (m), and k is the Von Karman constant (≈ 0.41). The displacement height and the canopy roughness lengths are estimated by simplified expressions as functions of canopy height, h (m): $d = 2h/3$, $z_{0M} = h/10$, and z_{0H} is taken as a fraction of z_{0M} ($z_{0H} = z_{0M}/7$) to account for less efficient transport of heat versus momentum near the canopy elements (Garratt & Hicks, 1973). The stability functions for heat, Ψ_H , and for momentum, Ψ_M , are obtained from Brutsaert (1999):

A) Unstable conditions:

$$\Psi_M(y) = \text{Ln}(a + y) - 3by^{1/3} + \frac{ba^{1/3}}{2} \text{Ln} \left[\frac{(1+x)^2}{(1-x+x^2)} \right] + 3^{1/2} ba^{1/3} \tan^{-1} [(2x-1)/3^{1/2}] + \Psi_0 \quad (\text{A2})$$

$$\Psi_H(y) = [(1-d)/n] \text{Ln}[(c+y^n)/c] \quad (\text{A3})$$

in which $x=(y/a)^{1/3}$, and $y=-(z-d)/L$. The symbol Ψ_0 denotes a constant of integration, given by $\Psi_0=(-\text{Ln}(a)+3^{1/2}ba^{1/3}\pi/6)$. The parameters a , b , c , d , and n are assigned constant values of 0.33, 0.41, 1.0, 0.33, 0.057, and 0.78, respectively (Brutsaert, 1999).

B) Stable conditions:

$$\Psi_M(y) = \Psi_H(y) = 5y \quad (\text{A4})$$

L is the Monin–Obukhov length (m) and is expressed as:

$$L = \frac{-u^*{}^3 \rho}{\text{kg} \left[\left(\frac{H}{T_a C_p} \right) + 0.61E \right]} \quad (\text{A5})$$

where u^* is the friction velocity, ρ is the air density (kg m^{-3}), g is the acceleration of gravity (m s^{-2}), C_p is the air specific heat at constant pressure ($\text{J kg}^{-1} \text{K}^{-1}$), H is the sensible heat flux, and E is the rate of surface evaporation ($\text{kg m}^{-2} \text{s}^{-1}$).

The aerodynamic resistance to heat transfer between point $z_{OM}+d$ and the reference height, r_a^a is written as a simplified form of Eq. (A1). Since the transport of heat and momentum is equally efficient, in this case $z_{OM}=z_{OH}$ (see Kustas & Norman, 1999a,b). Also, in this case $z_u=z_T$. Finally, r_a^a is given by the expression:

$$r_a^a = \frac{\left[\text{Ln} \left(\frac{z_u-d}{z_{OM}} \right) - \Psi_M \right] \left[\left[\text{Ln} \left(\frac{z_u-d}{z_{OM}} \right) - \Psi_H \right] \right]}{k^2 u} \quad (\text{A6})$$

Finally, the aerodynamic resistance to heat flow in the boundary layer immediately above the soil surface, r_a^s , is estimated from an empirical expression developed by Sauer et al. (1995) from extensive studies of this soil-surface resistance in a wind tunnel and beneath a corn canopy. This expression was modified and improved later by Kustas and Norman (1999a,b):

$$r_a^s = \frac{1}{0.0025(T_s - T_c)^{1/3} + 0.012u_s} \quad (\text{A7})$$

where u_s is the wind speed at height above the soil surface where the effect of soil surface roughness on the free wind movement can be neglected, z' (m s^{-1}) (Sauer et al., 1995). This wind speed is determined assuming a logarithmic wind profile in the air space above the soil:

$$u_s = u \left[\frac{\text{Ln} \left(\frac{z'}{z'_0} \right)}{\left[\text{Ln} \left(\frac{z_u}{z_0} \right) - \Psi_M \right]} \right] \quad (\text{A8})$$

where z'_0 is the soil roughness length. In this expression the displacement height was zero while stability corrections were really not used because of the close proximity to the soil surface (Sauer et al., 1995). Unlike in two-layer schemes, the exponential wind profile in the canopy air space is not applied in the patch approach.

References

- Anderson, M. C., Neale, C. M. U., Li, F., Norman, J. M., Kustas, W. P., Jayanthi, H., et al. (2004). Upscaling ground observations of vegetation water content, canopy height, and leaf area index during SMEX02 using aircraft and Landsat imagery. *Remote Sensing of Environment*, 92, 447–464.
- Anderson, M. C., Norman, J. M., Diak, G. R., Kustas, W. P., & Mecikalski, J. R. (1997). A two-source time-integrated model for estimating surface fluxes using thermal infrared remote sensing. *Remote Sensing of Environment*, 60, 195–216.
- Anderson, M. C., Norman, J. M., Kustas, W. P., Li, F., Prueger, J. H., & Mecikalski, J. R. (2005). Effects of vegetation clumping on two-source model predictions of surface energy fluxes from an agricultural landscape during SMACEX. *Journal of Hydrometeorology*, 6, 892–909.
- Berk, A., Anderson, G. P., Acharya, P. K., Chetwynd, J. H., Bernstein, L. S., Shettle, E. P., et al. (1999). *MODTRAN 4 User's Manual (Hascom AFB, MA: Air Force Research Laboratory, Space Vehicles Directorate, Air Force Materiel Command)*.
- Blyth, E. M., & Harding, R. J. (1995). Application of aggregation models to surface heat flux from the Sahelian tiger bush. *Agricultural and Forest Meteorology*, 72, 213–235.
- Brutsaert, W. (1999). Aspects of bulk atmospheric boundary layer similarity under free-convective conditions. *Reviews of Geophysics*, 37(4), 439–451.
- Bugbee, B., Droter, M., Monje, O., & Tanner, B. (1999). Evaluation and modification of commercial infrared-red transducers for leaf temperature measurement. *Advanced Space Resources*, 22, 1425–1434.
- Campbell, G. S., & Norman, J. M. (1998). *An introduction to environmental biophysics*. New York: Springer. 286 pp.
- Caselles, V., Sobrino, J. A., & Coll, C. (1992). A physical model for interpreting the land surface temperature obtained by remote sensors over incomplete canopies. *Remote Sensing of Environment*, 39, 203–211.
- Chehbouni, A., Nouvellon, Y., Kerr, Y. H., Moran, M. S., Watts, C., Prévot, L., et al. (2001). Directional effect on radiative surface temperature measurements over a semiarid grassland site. *Remote Sensing of Environment*, 76, 360–372.
- Chehbouni, A., Nouvellon, Y., Lhomme, J.-P., Watts, C., Boulet, G., Kerr, Y. H., et al. (2001). Estimation of surface sensible heat flux using dual angle observations of radiative surface temperature. *Agricultural and Forest Meteorology*, 108, 55–65.
- Choudhury, B. J., Idso, S. B., & Reginato, R. J. (1987). Analysis of an empirical model for soil heat flux under a growing wheat crop for estimating evaporation by an infrared-temperature based energy balance equation. *Agricultural and Forest Meteorology*, 39, 283–297.
- Choudhury, B., & Monteith, J. (1988). A four-layer model for the heat budget of homogeneous land surfaces. *Quarterly Journal of the Royal Meteorological Society*, 114, 373–398.
- Coll, C., Caselles, V., Galve, J. M., Valor, E., Niclòs, R., Sánchez, J. M., et al. (2005). Ground measurements for the validation of land surface temperatures derived from AATSR and MODIS data. *Remote Sensing of Environment*, 97, 288–300.
- Coll, C., Valor, E., Caselles, V., & Niclòs, R. (2003). Adjusted Normalized Emissivity Method for surface temperature and emissivity retrieval from optical and thermal infrared remote sensing data. *Journal of Geophysical Research*, 108. doi:10.1029/2003JD003688
- Foken, T., Wimmer, F., Mauder, M., Thomas, C., & Liebethal, C. (2006). Some aspects of the energy balance closure problem. *Atmospheric Chemistry and Physics*, 6, 4395–4402.
- François, C. (2002). The potential of directional radiometric temperatures for monitoring soil and leaf temperature and soil moisture status. *Remote Sensing of Environment*, 80, 122–133.
- François, C., Ottlé, C., & Prévot, L. (1997). Analytical parameterization of canopy directional emissivity and directional radiance in the thermal infrared. Application on the retrieval of soil and foliage temperatures using two directional measurements. *International Journal of Remote Sensing*, 18(12), 2587–2621.
- French, A. N., Jacob, F., Anderson, M. C., Kustas, W. P., Timmermans, W., Gieske, A., et al. (2005). Surface energy fluxes with the Advanced Spaceborne Thermal Emission and Reflection radiometer (ASTER) at the Iowa 2002 SMACEX site (USA). *Remote Sensing of Environment*, 99(1–2), 55–65.

- French, A. N., Schmugge, T. J., Kustas, W. P., Brubaker, K. L., & Prueger, J. (2003). Surface energy fluxes over El Reno Oklahoma, using high-resolution remotely sensed data. *Water Resources Research*, 39(6), 1164.
- Garratt, J. R., & Hicks, B. B. (1973). Momentum, heat and water vapour transfer to and from natural and artificial surfaces. *Quarterly Journal of the Royal Meteorological Society*, 99, 680–687.
- Hall, F., Huemmrich, K., Goetz, S., Sellers, P., & Nickerson, J. (1992). Satellite remote sensing of surface energy balance: Success, failures and unresolved issues in FIFE. *Journal of Geophysical Research*, 97, 19061–19089.
- Jia, L., Li, Z. -L., Menenti, M., Su, Z., Verhoef, W., & Wan, Z. (2003). A practical algorithm to infer soil and foliage component temperatures from bi-angular ATSR-2 data. *International Journal of Remote Sensing*, 24(23), 4739–4760.
- Jia, L., Su, Z., Van der Hurk, B., Menenti, M., Moene, A., De Bruin, H. A. R., et al. (2003). Estimation of sensible heat flux using the Surface Energy Balance System (SEBS) and ATSR measurements. *Physics and Chemistry of the Earth*, 28, 75–88.
- Kimes, D. S. (1983). Remote sensing of row crop structure and component temperatures using directional radiometric temperatures and inversion techniques. *Remote Sensing of Environment*, 13, 33–55.
- Kustas, W. P., & Norman, J. M. (1997). A two-source approach for estimating turbulent fluxes using multiple angle thermal infrared observations. *Water Resources Research*, 33(6), 1495–1508.
- Kustas, W. P., & Norman, J. M. (1999). Evaluation of soil and vegetation heat flux predictions using a simple two-source model with radiometric temperatures for partial canopy cover. *Agricultural and Forest Meteorology*, 94, 13–29.
- Kustas, W. P., & Norman, J. M. (1999). Reply to comments about the basic equations of dual-source vegetation-atmosphere models. *Agricultural and Forest Meteorology*, 94, 275–278.
- Kustas, W. P., & Norman, J. M. (2000). A two-source energy balance approach using directional radiometric temperature observations for sparse canopy covered surfaces. *Agronomie Journal*, 92, 847–854.
- Kustas, W. P., Norman, J. M., Schmugge, T. J., & Anderson, M. C. (2004). Mapping surface energy fluxes with radiometric temperature. Chapter 7. In D. Quattrochi & J. Luvall (Eds.), *Thermal Remote Sensing in Land Surface Processes* (pp. 205–253). Florida, USA: CRC Press Boca Raton Book Chapter.
- Lagouarde, J. P., Ballans, H., Moreau, P., Guyon, D., & Coraboeuf, D. (2000). Experimental study of brightness surface temperature angular variations of maritime pine (*Pinus pinaster*) stands. *Remote Sensing of Environment*, 72, 17–34.
- Lagouarde, J. P., Kerr, Y. H., & Brunet, Y. (1995). An experimental study of angular effects on surface temperature for various plant canopies and bare soils. *Agricultural and Forest Meteorology*, 77, 167–190.
- Lamaud, E., Ogée, J., Brunet, Y., & Berbigier, P. (2001). Validation of eddy flux measurements above the understorey of a pine forest. *Agricultural and Forest Meteorology*, 106, 187–203.
- Laubach, J., & Teichmann, U. (1999). Surface energy budget variability: A case study over grass with special regard to minor inhomogeneities in the source area. *Theoretical and Applied Climatology*, 62(1–2), 9–24.
- Lhomme, J. -P., & Chehbouni, A. (1999). Comments on dual-source vegetation-atmosphere transfer models. *Agricultural and Forest Meteorology*, 94, 269–273.
- Li, F., Kustas, W. P., Prueger, J. H., Neale, C. M. U., & Jackson, J. J. (2005). Utility of remote sensing based two-source energy balance model under low and high vegetation cover conditions. *Journal of Hydrometeorology*, 6(6), 878–891.
- Merlin, O., & Chehbouni, A. (2004). Different approaches in estimating heat flux using dual angle observations of radiative surface temperature. *International Journal of Remote Sensing*, 25(1), 275–289.
- Meyers, T., & Hollinger, P. (2004). An assessment of storage terms in the surface energy balance of maize and soybean. *Agricultural and Forest Meteorology*, 125, 105–115.
- Mira, M., Valor, E., Boluda, R., Caselles, V., & Coll, C. (in press). Influence of soil water content on the thermal infrared emissivity of bare soils. Implication for land surface temperature determination. *Journal of Geophysical Research*.
- Norman, J. M., Kustas, W., & Humes, K. (1995). A two-source approach for estimating soil and vegetation energy fluxes from observations of directional radiometric surface temperature. *Agricultural and Forest Meteorology*, 77, 263–293.
- Otterman, J., Brakke, T. W., & Susskind, J. (1992). A model for inferring canopy and underlying soil temperatures from multi-directional measurements. *Boundary-Layer Meteorology*, 61, 81–97.
- Prueger, J. H., Hatfield, J. L., Kustas, W. P., Hipps, L. E., & McPherson, I. (2005). Tower and aircraft eddy covariance measurements of water, energy and carbon fluxes during SMACEX. *Journal of Hydrometeorology*, 6(6).
- Rubio, E., Caselles, V., Coll, C., Valor, E., & Sospedra, F. (2003). Thermal infrared emissivities of natural surfaces: Improvements on the experimental set-up and new measurements. *International Journal of Remote Sensing*, 20(24), 5379–5390.
- Santanello, J. A., & Friedl, M. (2003). Diurnal covariation in soil heat flux and net radiation. *Journal of Applied Meteorology*, 42, 851–862.
- Sauer, T. J., Norman, J. M., Tanner, C. B., & Wilson, T. B. (1995). Measurement of heat and vapour transfer coefficients at the soil surface beneath a maize canopy using source plates. *Agricultural and Forest Meteorology*, 75, 161–189.
- Schmugge, T. J., Kustas, W. P., & Humes, K. S. (1998). Monitoring land surface fluxes using ASTER observations. *IEEE Transactions on Geoscience and Remote Sensing*, 36(5), 1421–1430.
- Sellers, P. J., Meeson, B. W., Hall, F. G., Asrar, G., Murphy, R. E., Schiffer, R. A., et al. (1995). Remote Sensing of the land surface for studies of global change: Models-algorithms-experiments. *Remote Sensing of Environment*, 51, 1–17.
- Shuttleworth, W., & Wallace, J. (1985). Evaporation from sparse crops: An energy combination theory. *Quarterly Journal of the Royal Meteorological Society*, 111, 1143–1162.
- Twine, T. E., Kustas, W. P., Norman, J. M., Cook, D. R., Houser, P. R., Meyers, T. P., et al. (2000). Correcting eddy-covariance flux underestimates over a grassland. *Agricultural and Forest Meteorology*, 103(3), 279–300.
- Valor, E., & Caselles, V. (1996). Mapping land surface emissivity from NDVI. Application to European, African and South-American areas. *Remote Sensing of Environment*, 57, 167–184.
- Wilson, K., Goldstein, A., Falge, E., Aubinet, M., Baldocchi, D., Berbigier, P., et al. (2002). Energy balance closure at FLUXNET sites. *Agricultural and Forest Meteorology*, 113, 223–243.
- Zhan, X., Kustas, W. P., & Humes, K. S. (1996). An intercomparison study on models of sensible heat flux over partial canopy surfaces with remotely sensed surface temperature. *Remote Sensing of Environment*, 58, 242–256.